Received: 27 January 2024 | Revised: 20 March 2024 | Accepted: 19 April 2024
DOI: 10.1002/jcc.27379

RESEARCH ARTICLE

Journal of COMPUTATIONAL CHEMISTRY WILEY

Restriction on molecular fluxionality by substitution: A case study for the 1,10-dicyanobullvalene

Bin-Bin Pei[1] | Hongjuan Yang[2] | Cai-Yue Gao[1] | Yuan Man[2] | Yonggang Yang[2] | Si-Dian Li[1]

[1]Nanocluster Laboratory, Institute of Molecular Science, Shanxi University, Taiyuan, China

[2]State Key Laboratory of Quantum Optics and Quantum Optics Devices, Institute of Laser Spectroscopy, Shanxi University, Taiyuan, China

Correspondence
Yonggang Yang, State Key Laboratory of Quantum Optics and Quantum Optics Devices, Institute of Laser Spectroscopy, Shanxi University, Taiyuan 030006, China.
Email: ygyang@sxu.edu.cn

Si-Dian Li, Nanocluster Laboratory, Institute of Molecular Science, Shanxi University, Taiyuan, 030006, China.
Email: lisidian@sxu.edu.cn

Funding information
National Natural Science Foundation of China, Grant/Award Numbers: 22373061, 21973057; 111 Project, Grant/Award Number: D18001; Hundred Talents Program of Shanxi Province

Abstract

We show herein that 1,10-dicyano substitution restricts the paragon fluxionality of bullvalene to just 14 isomers which isomerize along a single cycle. The restricted fluxionality of 1,10-dicyanobullvalene (DCB) is investigated by means of: (i) Bonding analyses of the isomer structures using the adaptive natural density partitioning (AdNDP). (ii) Quantum dynamical simulations of the isomerizations along the cyclic intrinsic reaction coordinate of the potential energy surface (PES). The PES possesses 14 equivalent potential wells supporting 14 isomers which are separated by 14 equivalent potential barriers supporting 14 transition states. Accordingly, at low temperatures, DCB appears as a hindered molecular rotor, without any delocalization of the wavefunction in the 14 potential wells, without any nuclear spin isomers, and with completely negligible tunneling. These results are compared and found to differ from those for molecular boron rotors. (iii) Born-Oppenheimer molecular dynamics (BOMD) simulations of thermally activated isomerizations. (iv) Calculations of the rate constants in the frame of transition state theory (TST) with reasonable agreement achieved with the BOMD results. (v) Simulations of the equilibration dynamics using rate equations for the isomerizations with TST rate coefficients. Accordingly, in the long-time limit, isomerizations of the 14 isomers, each with C_s symmetry, approach the "14 $C_s \rightarrow C_{7v}$" thermally averaged structure. This is a superposition of the 14 equally populated isomer structures with an overall C_{7v} symmetry. By extrapolation, the results for DCB yield working hypotheses for so far un-explored properties e.g. for the equilibration dynamics of $C_{10}H_{10}$.

KEYWORDS
1,10-dicyanobullvalene, bullvalene, equilibration, fluxionality, restriction

1 | INTRODUCTION

The fluxionality of bullvalene $C_{10}H_{10}$ is unequaled, and it remains challenging. On one hand, we already know many of its important properties, but on the other hand, there are many other properties which remain unexplored, even 60 years after its prediction by von Doering and Roth[1] and after its first synthesis by Schröder.[2,3] For example, bullvalene has $10!/3 = 1{,}209{,}600$ equivalent isomers which can isomerize along a network of $10!/(3 \times 14/3) = 259{,}200$ cyclic paths, with 14 isomers in each cycle in which each isomer is shared by three cycles and each arc is common to two different paths.[4] But it is unknown, for example, how the isomerizations yield equilibration, how long it will take to equilibrate, and how the thermally averaged structure would look like.[5]

Here we restrict the fluxionality of bullvalene by 1,10-dicyano substitution. The restricted fluxionality of the resulting 1,10-dicyanobullvalene (DCB) is still significant, but no longer exorbitant, namely it allows

14 equivalent isomers to isomerize along a single cyclic path, as illustrated in Figure 1. This allows us to investigate properties of DCB which remain unexplored for the parent bullvalene, such as the equilibration dynamics. Our investigation profits from experience of our previous studies on fluxional molecules and fluxional bonds.[6–13]

We note that an even more drastic restriction of bullvalene's isomerizations to just one isomerization of two equivalent isomers has been achieved by replacing the three CH groups of the "wheel" ABC of $C_{10}H_{10}$ shown in Figure 1 by just two or even by just a single CH group. These modifications generate the so-called barbaralane and semi-bullvalene (SBV) which have lent themselves to enormous numbers of illuminating experimental and theoretical investigations.[14–24]

The methods and the time-independent and time-dependent results for DCB are in Sections 2–4. Section 5 has a summary and the conclusions, with the results for DCB extrapolated to working hypotheses for so far unexplored properties of bullvalene.

2 | THEORETICAL PROCEDURE AND COMPUTATIONAL METHOD

Isomer structures (IS) and transition state (TS) structures of DCB in the electronic ground state were optimized at the hybrid density

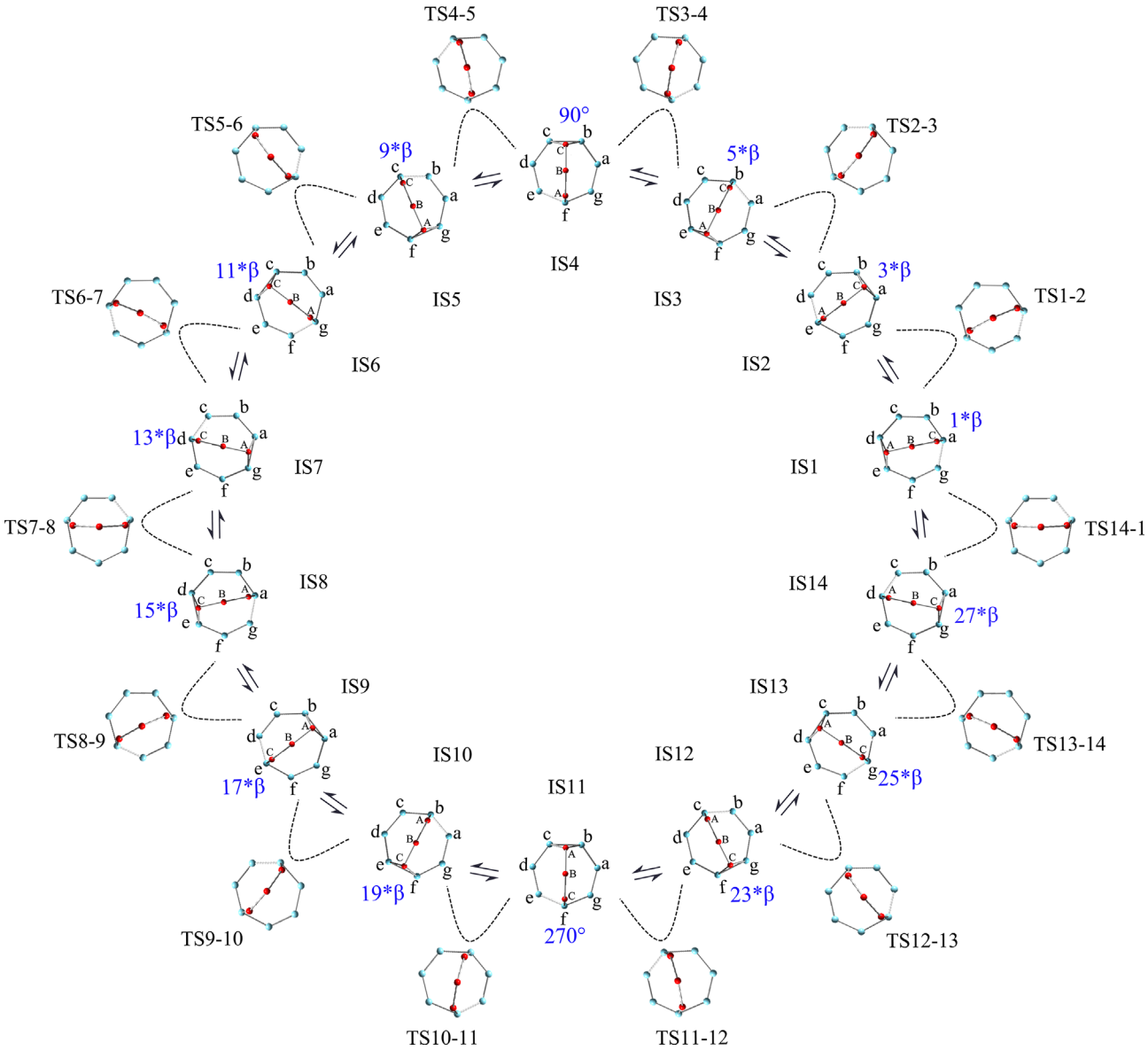

FIGURE 1 Cycle of 14 isomer structures IS1, IS2, ..., IS14 with 14 transition states TS1-2, TS2-3, ..., TS14-1 of bullvalene or 1,10-dicyanobullvalene (DCB). The top views of the ISi's appear as a "wheel" on top of the "bearing" with carbon nuclei A, B, C and a, b, c, ..., g, respectively, in accord with the "rotational operation" predicted in Reference [1]. In the case of DCB, the two cyano groups are attached to the carbon nuclei A and C. Bullvalene has 10!/(3 × 14/3) equivalent cycles, whereas DCB has just one cycle. The intrinsic reaction coordinates from IS1 via TS1-2 to IS2 and so forth. are indicated schematically, compare with Figure 2B. Isomerizations between neighboring ISi and IS$i+1$ are indicated by "⇌". The angles of the "wheel" with respect to the "bearing" are $\varphi_i = (2i-1) \times \beta$ for ISi, $i = 1, 2, ..., 14$, with $\beta = 360°/28$.

functional theory (DFT) level of PBE0 with the basis set of 6–311 + G (d).[25,26] Frequency calculations were performed to make sure that all the optimized structures are true ISs or TSs. All the PBE0 structural optimizations and additional coupled cluster CCSD(T) single-point calculations in this work were performed using the Gaussian 16 package and Molpro.[27–29] Detailed bonding analyses of the structures were performed using the adaptive natural density partitioning (AdNDP).[30,31] Born-Oppenheimer molecular dynamics simulation (BOMD) of DCB were performed using the CP2K program at temperatures ranging from 700 to 900 K.[32] The isomerization rate constants (k) are calculated by means of transition state theory (TST).[33,34]

3 | TIME-INDEPENDENT RESULTS

3.1 | Time-independent results for individual IS and TS structures

DCB has various close-lying isomers, see Figure S1. Here we consider DCB. Two equivalent ISs with C_s symmetry called ISi and ISj are shown in Figure 2A. Figure 2A also shows the other isomer ISj' obtained from the second fluctuating channel which lies 0.14 eV higher than ISi at CCSD(T) level, as shown in Figure 2B. The intrinsic reaction coordinates (IRC) from ISi via the transition state TS$i - j$ to ISj as well as from ISi via the transition state TS$i - j'$ to ISj' are shown in Figure 2B.

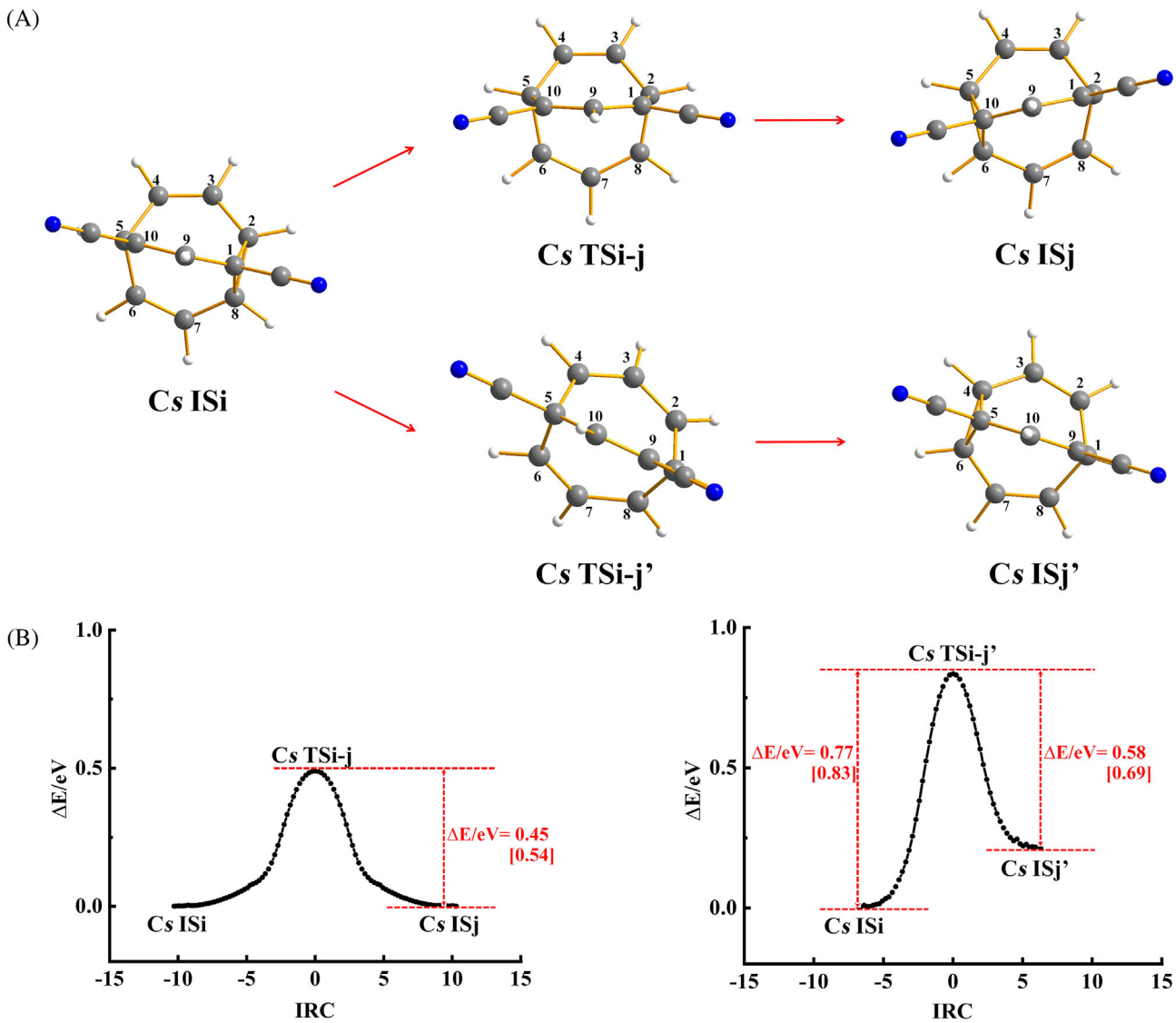

FIGURE 2 (A) Top views of the optimized isomer structures ISi, ISj, and ISj' and transition states TS$i - j$ and TS$i - j'$ of 1,10-dicyanobullvalene (DCB). (B) Intrinsic reaction coordinates (IRC) from ISi via TS$i - j$ to ISj and from ISi via TSi – j' to ISj', in units of $u^{1/2} \cdot a_0$. The values of the barrier heights of TS$i - j$ and TSi – j' and the energy of ISj relative to ISj' are obtained at the PBE0/6-311 + G(d) and CCSD(T)/6-311 + G(d) (in square brackets []) levels.

DCB possesses the lowest energy barrier obtained between any two isomers at the transition state TS$i-j$. The path IS$i \rightarrow$ TS$i-j \rightarrow$ ISj is, therefore, the preferred isomerization among various competing processes, as evidenced by detailed BOMD simulations presented later. Note that without the 1,10-dicyano substitution, the path IS$i \rightarrow$ TS$i-j' \rightarrow$ ISj' would be equivalent to the path IS$i \rightarrow$ TS$i-j \rightarrow$ ISj, as in the case of bullvalene where the isomer structures ISj and ISj' are equivalent. Turning the table, the 1,10-dicyano substitution supports the isomerization IS$i \rightarrow$ TS$i-j \rightarrow$ ISj between two equivalent isomers but blocks the alternative isomerization IS$i \rightarrow$ TS$i-j' \rightarrow$ ISj' to the third isomer. This kinetic blockade is due to the much high energy barrier (0.83 eV) of TS$i-j'$ compared to that (0.54 eV) of TS$i-j$ at CCSD(T). As a consequence, the $10!/(3 \times 14/3)$ isomerization cycles of bullvalene are restricted to a single cycle for DCB. For this restriction, DCB was chosen as the best candidate out of several other low-lying isomers, cf. Supporting information.

The calculated adaptive natural density partitioning (AdNDP) bonding patterns of ISi, ISj, and TS$i-j$ of DCB are shown in Figure 3. As anticipated, C_s IS DCB possesses 2 lone pair electrons on each N, 4 C—N 2c—2e π bonds, 24 2c-2e σ-bonds including 14 C—C σ single bonds, 2 C—N σ single bonds, and 8 C—H σ single bonds with the occupation numbers of ON = 1. 89–2.00 |e|, and 3 C—C 2c—2e π bonds with ON = 1. 93 |e|. C_s TS DCB possesses 2 lone pair electrons on each N, 4 C—N 2c—2e π bonds, 23 2c—2e σ-bonds including 13 C—C σ single bonds, 2 C—N σ single bonds, and 8 C—H σ single bonds with the occupation numbers of ON = 1. 93–2.00 |e|, 1 4c—2e σ-bonds on C1, C8 and C6, C10, and 1 2c—2e π bonds and 2 3c—2e π bonds with ON = 1. 91–1.96 |e|. AdNDP bonding analysis suggests that DCB isomerizes by rapid Cope rearrangements. Accordingly, DCB undergoes a concerted structural fluctuation involving one fluxional σ-bond (ISi (1 2c—2e σ) → TSij (1 4c—2e σ) → ISj (1 2c—2e σ)) and two fluxional π bonds (ISi (2 2c—2e π) → TS$i-j$ (2 3c—2e π) → ISj (2 2c—2e π)) which fluctuate in opposite directions simultaneously.

3.2 | Time-independent results for the interacting 14 ISs

DCB has altogether 14 equivalent isomer structures labeled as IS1, IS2, ..., IS14 or ISi, $i = 1, 2, ..., 14$. The IRC leads in a cycle from IS1 via TS1-2 to IS2, then from IS2 via TS2-3 to IS3, and so forth, and finally from IS14 via TS14-1 back to IS1. The cycle IS1 → TS1-2 → IS2 → TS2-3 → ... → IS14 → TS14-1 → IS1 is illustrated in Figure 1, with top views of the ISi and TS$i-i+1$. With these labels, the structures ISi, TS$i-j$, ISj shown in Figure 2A correspond to IS14, TS14-1 and IS1, respectively. For convenience, the carbon nuclei labeled as 1, 2, 3, 4, 5, 6, 7, 8, 9, 10 in Figure 2A are re-labeled as A, a, b, c, d, e, f, g, B, C, respectively in Figure 1. In this way, carbon nuclei (A, B, C) may be considered as a "wheel" which is rotating on top of the "bearing" consisting of seven carbon nuclei (a, b, ..., g). This type of "rotational operation" was already predicted for bullvalene.[1] The rotation angles of the wheel with respect to the bearing are $\varphi = (2i-1) \times \beta$ for ISi, $i = 1, 2, ..., 14$, with $\beta = 360°/28$.

All nuclear coordinates (X_i, Y_i, Z_i), $i = 1, 2, ..., 22$ of all 14 IS's and all 14 TS$i-i+1$, $i = 1, 2, ..., 14$ are listed in Table S2, respectively. For this purpose, we use a laboratory fixed right-handed system of

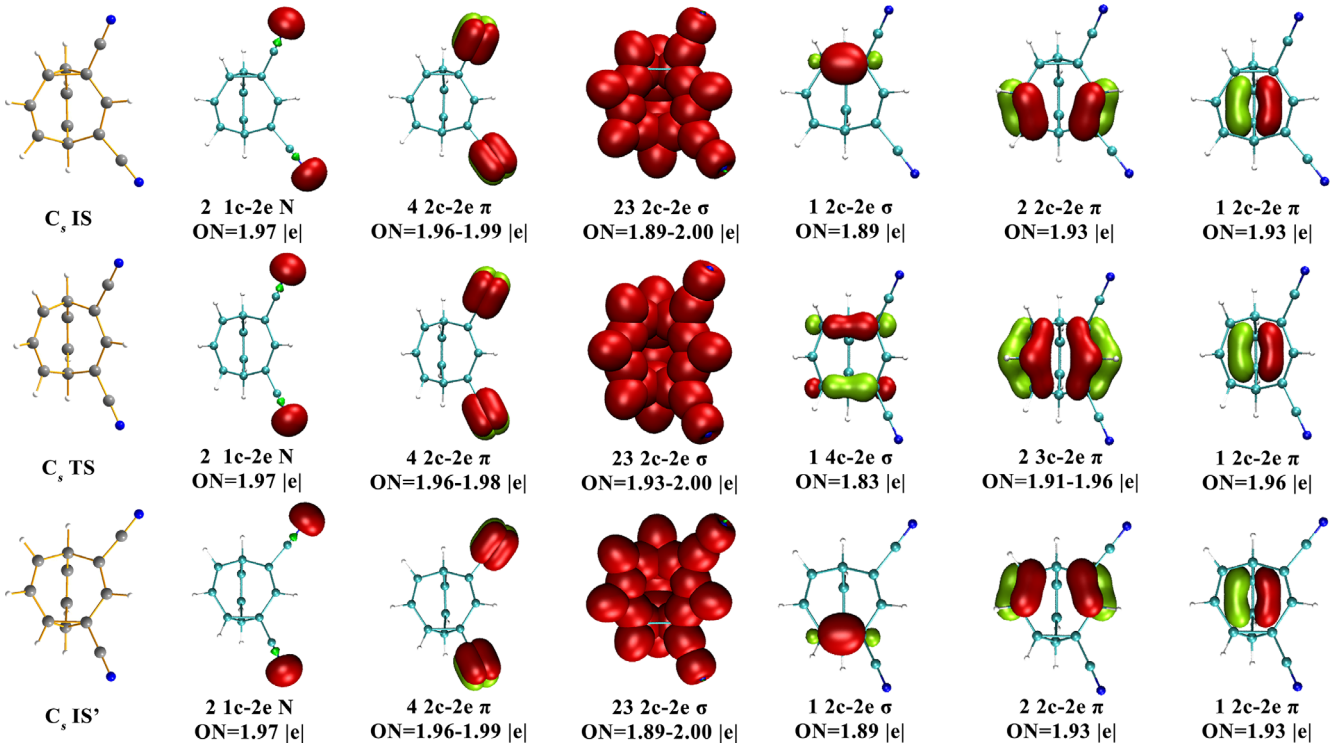

FIGURE 3 Adaptive natural density partitioning (AdNDP) bonding patterns of ISi, ISj, and TS$i-j$ of 1,10-dicyanobullvalene (DCB). The ON values represent the calculated occupation numbers of the corresponding bonds.

Cartesian coordinates. The origin is at the center of mass. For the specific isomer structure IS4, the C_s-symmetry plane is the *y*-*z*-plane, with the principal axis along the z-coordinate almost perfectly parallel to the C_BH_B bond that is, the z-axis serves as the rotation axis of the "wheel" (A, B, C) with respect to the "bearing" (a, b, c, ..., g). During the rotation of the "wheel" (A, B, C), the "bearing" (a, b, c, ..., g) undergoes slight deformations (below the graphical resolution of Figure 1). The values of the corresponding moments of inertia of the "wheel" and the "bearing" of the isomer structures are

$$I_w = \sum_{j=1}^{14} M_j \times \left(X_j^2 + Y_j^2\right) \text{ and}$$

$$I_b = \sum_{j=15}^{22} M_j \times \left(X_j^2 + Y_j^2\right), \text{ respectively.}$$

The reduced moment of inertia is $I_{IS} = \frac{I_w \times I_b}{I_w + I_b}$. Equivalent expressions hold for the reduced moment of inertia of the transition state I_{TS}. For the model below, we use the mean value, $I = 0.5\ (I_{IS} + I_{TS}) = 170.76\ \mu\text{Å}^2$.

The cycle IS1 → TS1-2 → IS2 → TS2-3 → ... → IS14 → TS14-1 shown in Figure 1 is mapped on the cyclic one-dimensional (1D) profile of the potential energy surface (PES) versus rotation angle φ for the rotation of the "wheel" (A, B, C) versus the "bearing" (a, b, c, ..., g), cf. Figure 4. The PES has 14 equivalent minima supporting the 14 equivalent IS1, IS2, ..., IS14. They are separated by the energy barriers for the 14 equivalent transition state structures TS1-2, TS2-3, ..., TS14-1. Isomerizations IS*i* ⇌ IS*i* + 1 between neighboring isomer structures are indicated by double arrows "⇌".

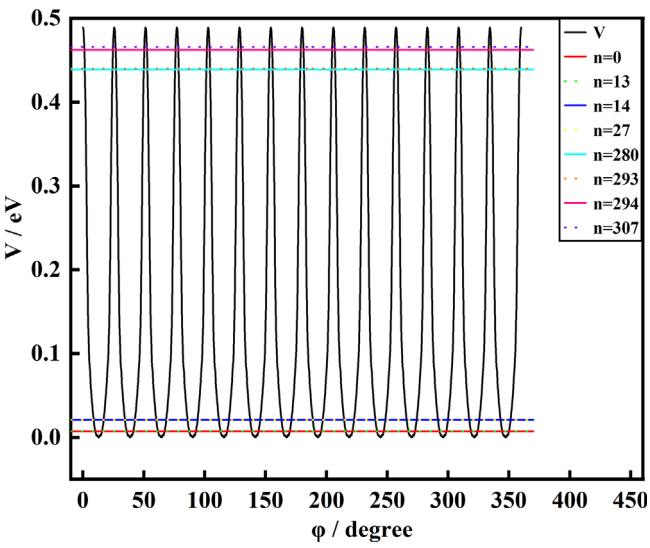

FIGURE 4 Cyclic one-dimensional profile of the potential energy surface (PES) versus rotation angle φ of the "wheel" (A, B, C) versus the "bearing" (a, b, c, ..., g) of 1,10-dicyanobullvalene (DCB), cf. Figure 1. The PES has 14 equivalent minima supporting the isomer structures IS1, IS2, ..., IS14 separated by the equivalent transition state structures TS1-2, TS2-3, ..., TS14-1. The profile of the PES from IS*i* via TS$i - i + 1$ to IS$i + 1$ corresponds to the intrinsic reaction coordinate (IRC) shown in Figure 2B. The horizontal lines illustrate bands ("tunneling quattuordecimets") of 14 near degenerate eigenenergies (E_n) of the intrinsic rotation versus *φ*, cf. Table S3.

The 1D PES *V*(*φ*) shown in Figure 4 lends itself for a simplistic 1D model of the coupled isomerizations IS1 ⇌ IS2 ⇌ IS3 ⇌ ... ⇌ IS13 ⇌ IS14 ⇌ IS1 mapped on the rotation of the "wheel" (A, B, C) versus the "bearing" (a, b, c, ..., g) along the rotation angle *φ*. The corresponding 1D Schrödinger equation.

$$\left[-\frac{\hbar^2}{2I}\frac{\partial^2}{\partial\varphi^2} + V(\varphi)\right]\psi_n(\varphi) = E_n\psi_n(\varphi) \tag{1}$$

with reduced moment of inertia *I* yields the corresponding rotational eigenenergies E_n. Figure 4 illustrates selected E_n's below the potential barriers by horizontal lines. They are grouped in sets of 14 eigenstates with near degenerate energies $E_0 \approx E_1 \approx \ldots \approx E_{13} < E_{14} \approx E_{15} \approx \ldots \approx E_{27} < \ldots < E_{294} \approx E_{295} \approx \ldots \approx E_{307}$, cf. Table S3. These sets of 14 eigenstates for the cyclic potential energy *V*(*φ*) with 14 equivalent minima may be called "tunneling quattuordecimets" (using the Latin number for 14), by analogy with the familiar "tunneling doublets" for cyclic potential energies *V*(*φ*) with two degenerate minima. In the case of DCB, they form extremely narrow bands of eigenstates. The band widths increase with mean energies of the bands. The highest band—actually the 22th—with mean energy just below the potential barriers has band width 0.0036 eV. By exponential extrapolation for the dependence of the tunneling splittings on the effective barrier heights, the bandwidth of the lowest energy band is about 5×10^{-13} eV—this is much below the graphical resolution of Figure 4. These splittings are even much below the interaction energies of the associated nuclear spins of the protons of the CH-bonds in DCB. As a consequence, DCB does not have any nuclear spin isomers—these would be represented by wavefunctions which are delocalized over all 14 minima of the PES. Instead DCB possesses localized eigenfunctions for the individual IS*i*'s. This property of DCB is in contrast with the molecular boron rotors such as B_{11}^-, B_{13}^+, B_{19}^+ which have nuclear spin isomers with delocalized wavefunctions covering all IS*i*'s.[6,10–13] This fundamental difference is a consequence of the much higher potential barriers and the much higher moment of inertia *I* of DCB compared to the boron rotors. Accordingly, DCB may be considered as "hindered molecular rotor".

4 | TIME-DEPENDENT RESULTS

Our investigation of the time-dependent aspects of the fluxionality of DCB has four parts labeled as IV.A–IV.D.

4.1 | Isomerization by tunneling

In the frame of the 1D-model developed in Section 3, the extremely small splittings of the energies of the 14 eigenstates in the lowest band ("quattuordecimet"), $\Delta E \approx 5 \times 10^{-13}$ eV imply the corresponding very long tunneling time,

$$\tau = h/\Delta E \approx 8\,\text{ms}. \quad (2)$$

Multi-D models take the couplings of tunneling along the intrinsic reaction coordinate IRC with complementary nuclear motions into account. These tend to slow down the tunneling that is, the 1D estimate (3) provides a lower limit to even longer tunneling times for multi-D models. Tunneling of DCB is in fact much slower than tunneling of semibullvalene at cryogenic temperatures[20] or tunneling of the boron rotors.[35] This is again a consequence of the much higher energy barrier and moment of inertia (or the corresponding reduced mass) of DCB compared to the boron rotors and semibullvalene.[16] As a resume, tunneling of the "hindered molecular rotor" DCB is negligible compared to thermally activated isomerizations, which will be considered in the next Section 4.2.

4.2 | BOMD simulations of thermally activated isomerizations

Molecular dynamics simulations of the fluxional isomerizations of DCB during 120 ps have been carried out for temperatures from 700 to 900 K. At these temperatures, the molecule would ultimately decompose, but this would take longer times. For reference, bullvalene is robust till 700 K.[36] The dynamics during the rather short temporal domain of 120 ps allow to monitor systematic trends which can be extrapolated to lower temperatures e. g. to room temperature where DCB is robust, but BOMD simulations would have to be carried out during much longer times which are beyond our computational resources.

Typical results for the time evolution of the root mean square deviation (RMSD) of the nuclear coordinates at time t from the configuration of the initial ($t = 0$) isomer IS1 obtained for a single trajectory are shown in Figure 5, for example, for $T = 900$ K. For the specific example, the initial IS1 apparently isomerizes to IS2, then back to IS1, then to IS14, ... and so forth. Analogous results for $T = 700$, 750, 800 K are presented in Figure S2. One may extrapolate that in the long-time limit, the isomerizations will visit all isomer structures with equal probabilities. The residence times for the isomer structures are shown in Table 1. The inverse of the mean values of the residence times yields an estimate of the rate of isomerization-here this is $k_{\text{BOMD}}(T = 900\text{ K}) = 1/\langle\tau\rangle = 1/2.665\text{ ps} = 0.375\text{ ps}^{-1}$. The results are shown in Figure 6.

4.3 | Transition state theory estimates of the rate coefficients for thermally activated isomerizations

Alternatively, we also calculate the rate constants of the isomerizations of DCB from ISi via TST$i - i + 1$ to IS$i + 1$ using TST, cf. Equation (3).

$$k_{\text{TST}}(T) = (k_B T/h) \times Q^{\text{TST}}/Q^{\text{IS}} \times \exp\left[-\left(E^{\text{TST}} - E^{\text{IS}}\right)/\text{RT}\right], \quad (3)$$

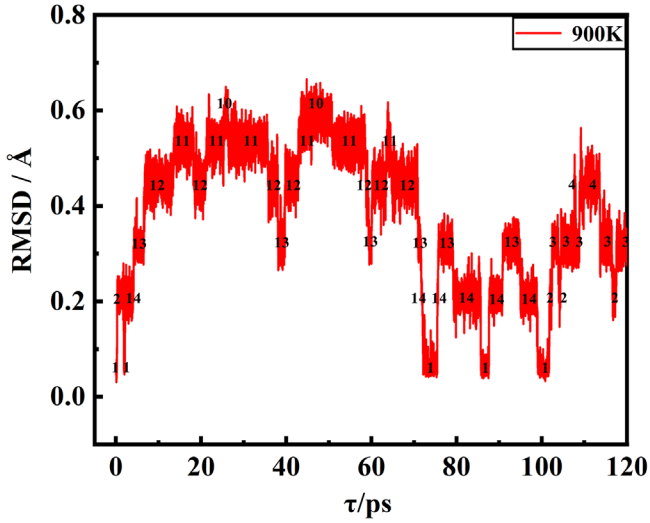

FIGURE 5 Born-Oppenheimer molecular dynamics (BOMD) simulation of the isomerizations of 1,10-dicyanobullvalene (DCB), by a single trajectory starting from isomer structure IS1 and visiting sequentially the ISi labeled by $i = 2, 1, 14, 13$, and so forth at 900 K. The root mean square deviation (RMSD) is the root mean square deviation of the nuclear coordinates at time t from the initial ($t = 0$) configuration.

TABLE 1 Residence times for isomer structures ISi of 1,10-dicyanobullvalene) during a Born-Oppenheimer molecular dynamics simulation visited by the trajectory starting at IS1 at $T = 900$ K[a].

900 K					
Structure	τ (ps)	Structure	τ (ps)	Structure	τ (ps)
IS14	0.15	IS13	1.26	IS12	3.10
IS14	0.18	IS3	1.36	IS13	3.37
IS1	0.21	IS2	1.52	IS14	3.86
IS12	0.29	IS1	1.75	IS13	4.01
IS4	0.31	IS14	1.96	IS11	4.21
IS11	0.44	IS12	2.00	IS4	4.65
IS2	0.49	IS13	2.33	IS11	4.86
IS2	0.51	IS3	2.36	IS12	5.96
IS3	0.53	IS1	2.43	IS14	6.32
IS13	0.71	IS12	2.61	IS12	6.75
IS13	0.73	IS3	2.78	IS10	6.96
IS2	0.74	IS14	2.79	IS11	7.75
IS10	0.92	IS12	2.82	IS11	9.13
IS11	1.08	IS1	3.08		

[a]The residence times correspond to the root mean square deviations of the trajectory shown in Figure 5. They are ordered from the shortest to increasing values. The mean value is $\langle\tau\rangle = 2.665$ ps.

where Q^{TST} and Q^{IS} are the vibrational partition functions of the TST and IS without vibrational zero- point energies (ZPEs) corrections considered, and $E^{\text{TST}} - E^{\text{IS}} = 0.27$ eV is the energy difference of the TST

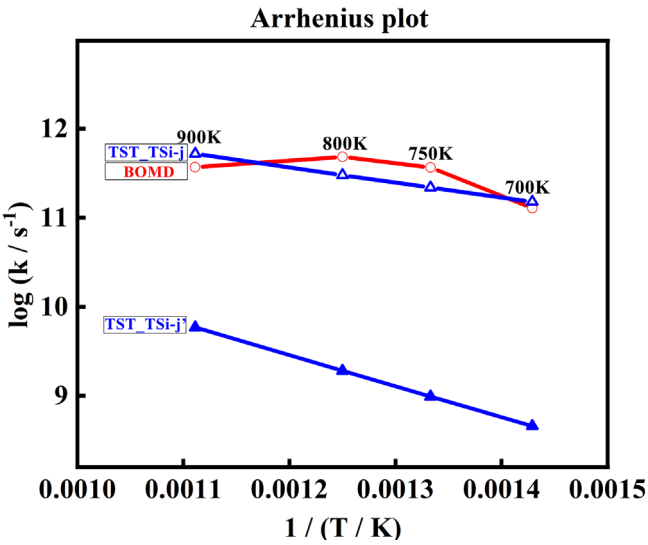

FIGURE 6 Comparison between the rate constants k for isomerizations IS$i \rightleftharpoons$ TS$i-j \rightleftharpoons$ ISj obtained from transition state theory (TST in blue) and BOMD simulations (in red) at different temperatures (T). For comparison, the much smaller TST rate constants k' for the competing isomerizations IS$i \rightleftharpoons$ TS$i-j' \rightleftharpoons$ ISj' are also shown in blue at the bottom, cf. Figure 2B.

and IS including the ZPEs. The results are also shown in Figure 6, in reasonable agreement with the BOMD results.

Figure 6 also shows the TST rate constants k'(T) for the competing isomerizations from ISi via TST$i-j'$ to ISj', cf. Figure 2. The much higher energy barrier of TST$i-j'$ compared to TSi-i + 1 implies that k'(T) < < k(T). For example, at 273 K (outside the range of Figure 2) we have $k'(273\text{ K}) = 16.8/\text{s} << k(273\text{ K}) = 4.79 \times 10^7/\text{s}$. This confirms the restriction of the fluxionality of DCB by dicyano substitution.

4.4 | Equilibration of DCB

The BOMD simulations presented in Section 4.2 assume that initially, at $t = 0$, DCB is prepared in a selective isomer ISj (in brief: the initial isomer) for example, in IS1 for the results shown in Figures 5 and 6 and in Table 1. The initial probabilities of observing the isomers IS1, ..., ISi, ..., IS14 (or in other words, the initial populations of the isomers) can thus be expressed in terms of Kronecker's symbol.

$$P_i(t=0) = \delta_{ij} = \begin{cases} 1 \text{ for } i=j \text{ (eg: } j=1); \\ 0 \text{ for } i \neq j. \end{cases} \tag{4}$$

Subsequently, the isomerizations of DCB induce transitions from the initial ISj to its nearest neighbors, IS$j+1$ or IS$j-1$, then to the next nearest neighbors IS$j+2$ or IS$j-2$, or back to ISj, and so forth. As a working hypothesis, in the long-time limit, the trajectories which simulate the isomerizations should visit all ISi's, ultimately with equal probabilities.

$$P_i(t \to \infty) \to 1/14. \tag{5}$$

This long-time limit of equal populations of all the equivalent isomers is in fact mandatory by fundamental laws of statistical thermodynamics. On the way from the initial to the final states, the population $P_j(t)$ of the selected initial ISj should decrease from its initial (=1) to the final (=1/14) value, whereas all other $P_i(t)$ should increase from 0 to 1/14.

This working hypothesis calls for calculations of the time evolutions of all $P_i(t)$ as solutions of the rate equations for the cyclic isomerizations of the ISi's,

$$\begin{aligned} dP_1/dt &= -2kP_1 + kP_{14} + kP_2, \\ dP_2/dt &= -2kP_2 + kP_1 + kP_3, \\ dP_3/dt &= -2kP_3 + kP_2 + kP_4, \\ &\ldots \\ dP_{13}/dt &= -2kP_{13} + kP_{12} + kP_{14}, \\ dP_{14}/dt &= -2kP_{14} + kP_{13} + kP_1 \end{aligned} \tag{6}$$

subject to the initial condition $P_i(t = 0) = \delta_{ij}$, with the rate coefficient k as determined in Section 4.3. It is convenient to rewrite equation (6) in matrix–vector notation.

$$\mathrm{d}\boldsymbol{P}/\mathrm{d}t = -k\,\boldsymbol{R}\,\boldsymbol{P} \tag{7}$$

with the "vector" of probabilities (or populations) $\mathbf{P} = (P_1, P_2, \ldots, P_{14})^T$ and the 14 × 14 "reaction matrix".

$$\mathbf{R} = \begin{pmatrix} 2 & -1 & & & & & -1 \\ -1 & 2 & -1 & & & & \\ & -1 & 2 & -1 & & & \\ & & & \ddots & & & \\ & & & -1 & 2 & -1 & \\ & & & & -1 & 2 & -1 \\ -1 & & & & & -1 & 2 \end{pmatrix}. \tag{8}$$

The special form of **R** guarantees normalization,

$$\sum_{m=1}^{14} P_m(t) = 1 \tag{9}$$

because,

$$d\left(\sum_{m=1}^{14} P_m\right)/\mathrm{d}t = -k\sum_{m=1}^{14}\sum_{n=1}^{14} R_{mn}P_n = 0. \tag{10}$$

The solution of the rate equations is obtained by diagonalization of the reaction matrix.

$$\boldsymbol{RU} = \boldsymbol{UD} \tag{11}$$

with unitary matrix **U** and with diagonal matrix.

$$\mathbf{D} = \begin{pmatrix} d_1 & & & & \\ & d_2 & & & \\ & & \ddots & & \\ & & & d_{13} & \\ & & & & d_{14} \end{pmatrix} \tag{12}$$

The solution of Equation (11) can be adapted from the analytical solution for the diagonalization of the isomorphous Hückel matrix for a cyclic aromatic hydrocarbon molecule with 14 equivalent $2p_z$-orbitals.[37] Accordingly, the diagonal elements are.

$$d_m = 2\{1 - \cos[(m-1) \times 2\pi/14]\} \tag{13}$$

or re-ordered with ascending values.

$$(d_1, d_2, \ldots, d_{14}) = (0.00, 0.20, 0.20, 0.75, 0.75, 1.55, 1.55, 2.44, 2.44, 3.24, 3.24, 3.80, 3.80, 4.00) \tag{14}$$

The d_m are associated with the elements U_{mn} of the unitary matrix **U**. For example, the matrix elements U_{m1} associated with the lowest eigenvalue $d_1 = 0.00$ are all equal,

$$U_{n1} = 1/\sqrt{14} \text{ for } n = 1, 2, \ldots, 14. \tag{15}$$

The general solution of the rate equations is obtained in terms of the elements of the matrices **D** and **U** as.

$$P_{i(t)} = \sum_{m=1}^{14} \sum_{n=1}^{14} U_{im} e^{-kd_m t} U_{nm} P_n(t=0). \tag{16}$$

For the special case $P_n(t = 0) = \delta_{nj}$ of the exclusive initial population of ISj, (cf. equation (4)) this simplifies to

$$P_i(t) = \sum_{m=1}^{14} U_{im}\, e^{-kd_m t} U_{jm}. \tag{17}$$

As an example, for the initial IS7, the time evolutions of the populations $P_i(t)$ of all isomer structures ISi at $T = 800$ K with $k = 0.302$/ps are illustrated in Figure 7A.

The numerical simulations of the time evolutions of the populations $P_i(t)$ of ISi confirm the conjectures based on the BOMD simulations in Section 4.2. In particular, in the long time limit, all exponentials in Equation (16) decay to zero, except the first one, since $\exp(-k\, d_1\, t) = \exp(0) = 1$. This implies equilibration.

$$P_i(t \to \infty) \to U_{i1}\, U_{j1} = 1/14 \tag{18}$$

in accord with Equation (5). The long-time approach to equilibrium is determined by the exponential in Equation (16) with the slowest decay that is, by $\exp(-k\, d_2\, t)$. In practice, one may say that equilibrium has been reached "essentially" if $\exp(-k\, d_2\, t)$ has decreased below some reasonable limit, say $\exp(-k\, d_2\, t) < \varepsilon = 0.01$ for

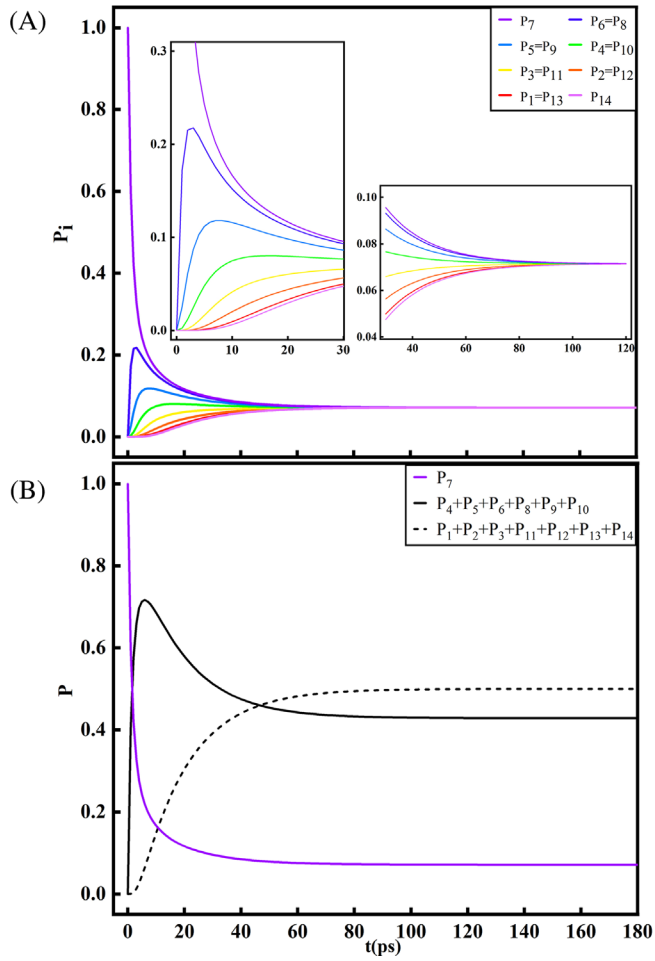

FIGURE 7 (A) Time evolutions of the populations $P_i(t)$ of the isomer structures ISi starting from initial preparation of DCB in ISj, $j = 7$ at $T = 800$ K. (B) Time evolutions of the populations of three groups of isomers, (i) the initial ISj = IS7, (ii) its six close neighbors ISi, $i = 4,5,6,8,9,10$ and (iii) the remaining more distant isomers ISi, $i = 1,2,3,11,12,13,14$. Group (ii) exhibits overshooting above the final equilibrium.

$$t > t_\varepsilon = -\ln \varepsilon/(k\, d_2). \tag{19}$$

For example, for the present application of the isomerizations of DCB with rate coefficients $k(T) = 1.50 \times 10^{11}$, 3.02×10^{11}, 5.29×10^{11}/s at temperatures $T = 700$, 800, and 900 K, the times for equilibration are $t_{\varepsilon=0.01}(T) = 153$, 76, and 43 ps, respectively. For comparison, at 273 K, $k(273\text{ K}) = 4.79 \times 10^7$/s and $t_{\varepsilon=0.01}(T) = 0.48$ μs.

Figure 7 also reveals additional phenomena, or rules during equilibration. These rules depend on the "distance" between the isomers ISi from the initial ISj. Here the "distance" depends on the arc between ISi and ISj on the circle of isomerizations illustrated in Figure 1. It is proportional to the minimum number of elementary isomerizations which transform ISj into ISi. For example, for the initial ISj = IS7, its nearest neighbors IS6 and IS8 have the closest distance to IS7, whereas the "opposite" IS14 has the largest distance from IS7.

First, Figure 7 reveals the "rule of hierarchy" of the populations of the isomers. Accordingly, the population $P_j(t)$ of the initial isomer ISj (cf. Equation (4)) remains always dominant,

$$P_j(t) > P_i(t) \text{ for } i \neq j. \tag{20}$$

Furthermore,

$$P_i(t) > P_k(t), \tag{21}$$

if isomer ISi is closer to the initial ISj than isomer ISk. Explicitly, for ISj = IS7, we have

$$\begin{aligned} P_7(t) > P_6(t) = P_8(t) > P_5(t) = P_9(t) > P_4(t) = P_{10}(t) > P_3(t) \\ = P_{11}(t) > P_2(t) = P_{12}(t) > P_1(t) = P_{13}(t) > P_{14}(t). \end{aligned} \tag{22}$$

This rule can be rationalized by the sequence of isomerizations which start from the initial ISj to its nearest neighbors IS$j+1$ and IS$j-1$, then to the next nearest neighbors IS$j+2$ and IS$j-2$, and so forth.

Second, Figure 7 reveals the "rule of symmetry" that is,

$$P_i(t) = P_k(t) \tag{23}$$

if isomers ISi and ISk have the same distance from the initial ISj, cf. Equation (22). This rule can be rationalized by the equivalence of clockwise and counterclockwise rotations of the "wheel" versus the "bearing" along the circle of isomerizations illustrated in Figure 1.

Third, Figure 7 reveals the "rule of overshooting" of the populations of the close neighbors of the initial isomer. Explicitly, all isomers can be assigned to three groups:

1. The initial isomer ISj (here: IS7)
2. Its close neighbors ISi. These yield transient populations which "overshoot" the equilibrium value. Here ISi = IS4, IS5, IS6, IS8, IS9, IS10 yield transient populations $P_i(t) > 1/14$ at sufficiently large times t. Those $P_i(t)$ pass through a rather early temporal maximum before the long-time approach to equilibrium.
3. The remaining isomers ISk at large distances from the initial ISj. Their populations increase monotonously to equilibrium, $P_k(t) < 1/14$.

This rule can be rationalized by the fact that isomers ISi can isomerize in two directions. Isomerizations in the direction away from the initial ISj contribute to populations of isomers at ever larger distances from the initial isomer. Isomerizations in the direction towards the initial ISj contribute to transient accumulation of populations of isomers close to the initial isomer, causing "overshooting. The populations of the isomers in groups (i), (ii) and (iii) are illustrated in Figure 7B, with clear demonstration of the phenomenon of overshooting of the isomers in group (ii) close to the initial ISj.

Equilibration by isomerization of all 14 isomers of DCB has important consequences for the thermally averaged structure and symmetry. The superposition of the structures of all 14 ISi's, each of them with C_s symmetry, is illustrated with rainbow colors in Figure 8B. The symmetry of this thermally averaged structure is C_{7v}. In brief, equilibration raises the symmetry of the 14 ISi's according to 14 $C_s \rightarrow C_{7v}$.

The C_{7v} structure of DCB at equilibrium is anticipated to have a ^{1}H NMR spectrum with two sets of inequivalent hydrogen atoms in the ratio of $n_{(a+b+c+d+e+f+g)}$: n_B = 7:1 (cf. Figure 1), in contrast to bullvalene $C_{10}H_{10}$ which is known to exhibit only one ^{1}H NMR signal above 120°C.[36] This reminds of the rise of symmetry of the boron rotors from multiple global minimum structures to unified quantum mechanical structures, for example, 18 $C_{2h} \rightarrow D_{9d}$ for La-[B_2@B_{18}]-La.[12] There is, however, an important difference between the two applications: The unified quantum mechanical structures of the boron rotors are for nuclear spin isomers with wavefunctions delocalized coherently over all equivalent global minimum structures. In contrast, the present DCB does not possess any nuclear spin isomers, and its thermally averaged structure is obtained as incoherent superposition of the isomer structures.

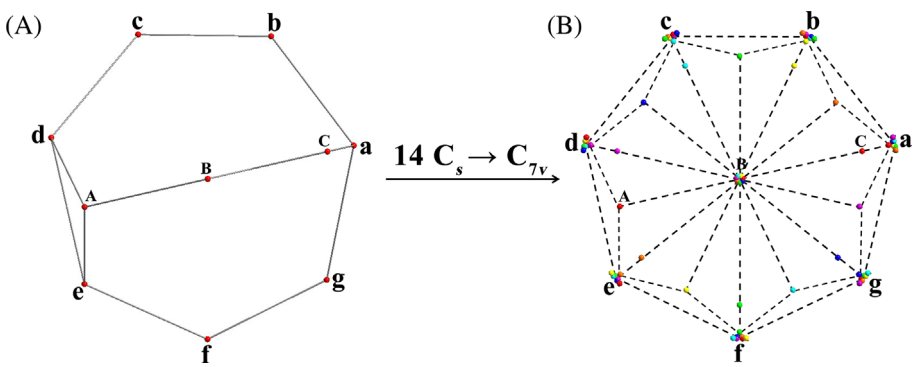

FIGURE 8 (A) Isomer structure IS1 of 1,10-dicyanobullvalene (DCB) illustrated by the positions of 10 carbon nuclei labeled as A, B, and C for the "wheel" and a, b, c, d, e, f, and g for the "bearing", cf. Figure 1. Figure 1 illustrates altogether 14 equivalent ISi, i = 1, 2, ..., 14, all of them with C_s symmetry. (B) The thermally averaged structure of DCB illustrated as rainbow-colored superposition of the structures of ISi, i = 1, 2, ..., 14 [IS1 (red), IS2(orange), IS3(yellow), IS4(green), IS5(cyan), IS6(blue), and IS7(purple), with IS8-IS14 overlapped with IS1-IS7]. A, B, and C in (B) represent the positions of the corresponding groups in IS1 in (A). The symbol "14 $C_s \rightarrow C_{7v}$" means that the superposition of 14 ISi, each with C_s symmetry, yields the thermally averaged structure with C_{7v} symmetry.

5 | CONCLUSIONS

Restriction of the paragon fluxionality of bullvalene by 1,10-dicyano substitution allows to investigate a broad variety of properties of DCB. These yield working hypotheses for corresponding properties of the parent bullvalene which cannot (yet) be investigated with the available methods and techniques.

First, the energy barriers between any two neighboring isomers and the reduced moment of inertia for the rotation of the "wheel" versus the "bearing" of DCB are so large that tunneling is entirely negligible. At low temperature, DCB appears, therefore, as frozen molecular rotor. The corresponding rotational energies are grouped into extremely narrow bands with tunneling splittings much below the interaction energies of nuclear spins. Consequently, DCB does not possess any nuclear spin isomers, and the wavefunctions are localized for the individual isomers instead of being delocalized over all isomer structures. The corresponding energy barriers of bullvalene are even higher than for DCB. The reference DCB suggests, therefore, the working hypothesis that bullvalene does not possess any nuclear spin isomers, either. This is non-trivial since $^{12}C_{10}H_{10}$ has 10 protons with nuclear spin ½ (in units of ħ). These might add up to total values of nuclear spins $I = 0, 1, \ldots, 5$. Thus one might speculate that $^{12}C_{10}H_{10}$ should have total molecular wavefunctions labeled by $I = 0, 1, \ldots, 4$ or 5. This possibility is ruled out, however, by the present results for DCB. The non-existence of nuclear spin isomers of DCB and bullvalene is entirely different from the boron rotors such as B_{11}^-, B_{13}^+, B_{19}^+ which possess nuclear spin isomers and delocalized wavefunctions because they isomerize via much lower energy barriers and with much lower reduced moments of inertia.[6]

Second, the present equilibration dynamics of DCB suggests, as working hypothesis, analogous phenomena for bullvalene. Thus, if bullvalene is prepared in one of its isomers, say in IS*j*, one should assign "distances" between IS*j* and the other 1,209,600–1 isomers IS*i* which depend on the length of the shortest isomerization path from the initial IS*i* to IS*j*. This length is proportional to the smallest number of elementary isomerizations which transform the initial IS*j* to the target ISi. The path must be determined on the rather complex graph for the 259,200 cyclic isomerization paths which has been described in the Introduction, adapted from Reference [4]. As a working hypothesis, the three rules of hierarchy, symmetry and overshooting during equilibration of DCB (cf. Equations (20)–(23)) should also apply to bullvalene. However, numerical simulations and analyses would be challenging. They would require the solution of the corresponding 1,209,600 coupled rate equations for all ISi, analogous to Equations (7). The underlying 1,209,600 × 1,209,600 reaction matrix **R** is still unknown, however, and we are not aware of any recipe for generating **R**. Its diagonalization (analogous to Equations (8)–(17)) appears as another formidable task.

In any case, the example of DCB shows that at (still unknown) rather long times, isomerizations yield equal populations of all isomers. The corresponding thermally averaged structure is the superposition of all individual isomer structures. In the case of DCB it has C_{7v} symmetry, which is "higher" (i.e. it has more symmetry elements) than the C_s symmetry of the 14 individual isomers, in brief 14 $C_s \rightarrow C_{7v}$, cf. Figure 8. By extrapolation, if bullvalene could be prepared in a single isomer, then a rather long series of isomerizations should yield the thermally averaged structure 1,209,600 $C_{3v} \rightarrow$ X with higher but still unknown (possibly I_h?) symmetry.

ACKNOWLEDGMENTS

One of us (Man) thanks Professor G. Buntkowsky (Darmstadt) for stimulating in-depth advice on the NMR spectra of bullvalene.[4] This work was financially supported by the National Natural Science Foundation of China (22373061 and 21973057 to Li), the 111 Project (Grant No. D18001 to Man), and the Hundred Talents Program of Shanxi Province (to Man).

DATA AVAILABILITY STATEMENT

The data that support the findings of this study are available from the corresponding author upon reasonable request.

ORCID

Si-Dian Li https://orcid.org/0000-0001-5666-0591

REFERENCES

[1] W. V. E. Doering, W. Roth, *Tetrahedron* **1963**, *19*, 715.
[2] G. Schröder, *Chem. Ber.* **1964**, *97*, 3140.
[3] R. Merényi, J. F. M. Oth, G. Schröder, *Chem. Ber.* **1964**, *97*, 3150.
[4] J. F. M. Oth, K. Müllen, J.-M. Gilles, G. Schröder, *Helv. Chim. Acta* **1974**, *57*, 1415.
[5] A. D. Ault, *Chem. Educ.* **2001**, *78*, 924.
[6] Y. Yang, D. Jia, Y.-J. Wang, H.-J. Zhai, Y. Man, S.-D. Li, *Nanoscale* **2017**, *9*, 1443.
[7] M. Yan, H. R. Li, X. Y. Zhao, X. Q. Lu, Y. W. Mu, H. G. Lu, S. D. Li, *J. Comput. Chem.* **2019**, *40*, 966.
[8] M. Yan, H. R. Li, X. X. Tian, Y. W. Mu, H. G. Lu, S. D. Li, *J. Comput. Chem.* **2019**, *40*, 1227.
[9] Y.-Y. Ma, M. Yan, H.-R. Li, Y.-B. Wu, X.-X. Tian, H.-G. Lu, S.-D. Li, *Sci. Rep.* **2019**, *9*, 17074.
[10] T. Grohmann, J. Manz, *Mol. Phys.* **2018**, *116*, 2538.
[11] T. Grohmann, D. Haase, D. Jia, J. Manz, Y. Yang, *J. Chem. Phys.* **2018**, *149*, 184302.
[12] X.-Q. Lu, Y. Man, V. Ruß, Y. Xu, Y. Yang, S.-D. Li, *Phys. Chem. Chem. Phys.* **2021**, *23*, 19146.
[13] Y. Xu, H. Wang, Y. Yang, C. Li, L. Xiao, S. Jia, *RSC Adv.* **2021**, *11*, 3613.
[14] H. E. Zimmerman, G. L. Grunewald, *J. Am. Chem. Soc.* **1966**, *88*, 183.
[15] A. K. Cheng, F. A. L. Anet, J. Mioduski, J. Meinwald, *J. Am. Chem. Soc.* **1974**, *96*, 2887.
[16] K. Bergmann, S. Görtler, J. Manz, H. Quast, *J. Am. Chem. Soc.* **1993**, *115*, 1490.
[17] G. E. Herberich, H. W. Marx, S. Moss, P. von Rague' Schleyer, T. Wagner, *Chem. A: Eur. J. Dermatol.* **1996**, *2*, 458.
[18] M. Garavelli, F. Bernardi, A. Cembran, O. Castano, L. M. Frutos, M. Merchán, M. Olivucci, *J. Am. Chem. Soc.* **2002**, *124*, 13770.
[19] D. A. Hrovat, E. C. Brown, R. V. Williams, H. Quast, W. T. Borden, *J. Org. Chem.* **2005**, *70*, 2627.
[20] X. Zhang, D. A. Hrovat, W. T. Borden, *Org. Lett.* **2010**, *12*, 2798.
[21] D. Andrae, I. Barth, T. Bredtmann, H. C. Hege, J. Manz, F. Marquardt, B. Paulus, *J. Phys. Chem. B* **2011**, *115*, 5476.
[22] T. Bredtmann, J. Manz, *Angew. Chem. Int. Ed.* **2011**, *50*, 12652.
[23] T. Bredtmann, D. J. Diestler, S.-D. Li, J. Manz, J. F. Pérez-Torres, W.-J. Tian, Y.-B. Wu, Y. Yang, H.-J. Zhai, *Phys. Chem. Chem. Phys.* **2015**, *17*, 29421.

[24] T. Bredtmann, J. Manz, J.-M. Zhao, *J. Phys. Chem. A* **2016**, *120*, 3142.
[25] C. Adamo, V. Barone, *J. Chem. Phys.* **1999**, *110*, 6158.
[26] R. Krishnan, J. S. Binkley, R. Seeger, J. A. Pople, *J. Chem. Phys.* **1980**, *72*, 650.
[27] G. D. Purvis, R. J. Bartlett, *J. Chem. Phys.* **1982**, *76*, 1910.
[28] M. J. Frisch, G. W. Trucks, H. B. Schlegel, G. E. Scuseria, M. A. Robb, J. R. Cheeseman, G. Scalmani, V. Barone, G. A. Petersson, H. Nakatsuji, X. Li, M. Caricato, A. V. Marenich, J. Bloino, B. G. Janesko, R. Gomperts, B. Mennucci, H. P. Hratchian, J. V. Ortiz, A. F. Izmaylov, J. L. Sonnenberg, D. Williams-Young, F. Ding, F. Lipparini, F. Egidi, J. Goings, B. Peng, A. Petrone, T. Henderson, D. Ranasinghe, V. G. Zakrzewski, J. Gao, N. Rega, G. Zheng, W. Liang, M. Hada, M. Ehara, K. Toyota, R. Fukuda, J. Hasegawa, M. Ishida, T. Nakajima, Y. Honda, O. Kitao, H. Nakai, T. Vreven, K. Throssell, J. A. Montgomery Jr., J. E. Peralta, F. Ogliaro, M. J. Bearpark, J. J. Heyd, E. N. Brothers, K. N. Kudin, V. N. Staroverov, T. A. Keith, R. Kobayashi, J. Normand, K. Raghavachari, A. P. Rendell, J. C. Burant, S. S. Iyengar, J. Tomasi, M. Cossi, J. M. Millam, M. Klene, C. Adamo, R. Cammi, J. W. Ochterski, R. L. Martin, K. Morokuma, O. Farkas, J. B. Foresman, D. J. Fox, C. T. Wallingford, Gaussian, Inc, *Revision A.03*, Gaussian Inc., Wallingford, CT **2016**.
[29] H. J. Werner, P. J. Knowles, G. Knizia, F. R. Manby, M. Schütz, *WIREs Comput. Mol. Sci.* **2012**, *2*, 242.
[30] D. Y. Zubarev, A. I. Boldyrev, *Phys. Chem. Chem. Phys.* **2008**, *10*, 5207.
[31] N. V. Tkachenko, A. I. Boldyrev, *Phys. Chem. Chem. Phys.* **2019**, *21*, 9590.
[32] J. VandeVondele, M. Krack, F. Mohamed, M. Parrinello, T. Chassaing, J. Hutter, *Comput. Phys. Commun.* **2005**, *167*, 103.
[33] K. Laidler, *Chemical Kinetics*, 3rd ed., Harper & Row Publ, New York **1987**.
[34] B. Peters, *Reaction Rate Theory and Rare Events*, Elsevier, Amsterdom **2017**.
[35] H. Yang, Y. Man, H. Wang, Y. Yang, *Chem. Phys.* **2022**, *562*, 11659.
[36] G. Schröder, J. F. M. Oth, R. Merényi, *Angew. Chem. Int. Ed. Engl.* **1965**, *4*, 752.
[37] E. Heilbronner, H. Bock, *Das HMO-Modell und seine Anwendungen*, 2nd. ed., Verlag Chemie, Weinheim **1965**.

SUPPORTING INFORMATION

Additional supporting information can be found online in the Supporting Information section at the end of this article.

How to cite this article: B.-B. Pei, H. Yang, C.-Y. Gao, Y. Man, Y. Yang, S.-D. Li, *J. Comput. Chem.* **2024**, 1. https://doi.org/10.1002/jcc.27379